Accepted Manuscript

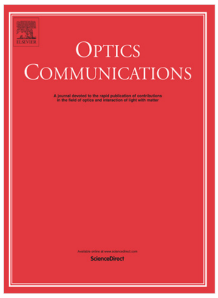

Broadband phase shift engineering for terahertz waves based on dielectric metasurface

Qianyi Mu, Hengzhi Lin, Fei Fan, Jierong Cheng, Xianghui Wang, Shengjiang Chang

PII: S0030-4018(18)30914-3
DOI: https://doi.org/10.1016/j.optcom.2018.10.039
Reference: OPTICS 23556

To appear in: *Optics Communications*

Received date : 30 July 2018
Revised date : 9 October 2018
Accepted date : 22 October 2018

Broadband phase shift engineering for terahertz waves based on dielectric metasurface

Qianyi Mu[1], Hengzhi Lin[1], Fei Fan[1, 3, *], Jierong Cheng[1], Xianghui Wang[1], Shengjiang Chang[1,2,**]

[1] *Institute of Modern Optics, Nankai University, Tianjin 300071, China*

[2] *Tianjin Key Laboratory of Optoelectronic Sensor and Network Technology, Tianjin 300350, China*

[3] *State Key Laboratory of Applied Optics, Changchun Institute of Optics, Fine Mechanics and Physics, Chinese Academy of Sciences, Changchun 130033, China*

Corresponding author: [*]fanfei_gao@126.com

[**]sjchang@nankai.edu.cn

Abstract: Broadband terahertz (THz) phase shift engineering and zero-dispersion waveplates based on dielectric metasurface have been investigated, of which structure is a periodical rectangular scattering units on silicon substrates. By designing proper geometric parameters of metasurface structure, the value, dispersion and bandwidth of the phase shift curves can be effectively manipulated. Based on this, the broadband half waveplate (HWP) and quarter waveplate (QWP) have been designed and fabricated. The experimental results show that the HWP can work in the broad range of 0.7-1.35 THz with the polarization conversion ratio (PCR) of close to 100% and the transmission of over 70%. And the QWP can operate in the range of 0.7~0.85THz with the PCR of over 90% and the transmission of over 70%. The method of phase shift engineering based on dielectric metasurfaces and these broadband zero-dispersion waveplates have great potential in promoting the performance of THz application systems.

Key words: Terahertz; Subwavelength structure; Metasurface; Dispersion control; Waveplate

1. Introduction

Terahertz (THz) radiation is electromagnetic radiation whose frequency lies 0.1 to 10 THz between the microwave and infrared regions. THz technology has broad application prospects in fields such as spectral detection [1], sensing [2], imaging detection [3] and wireless communication [4]. THz modulators [5], filters [6], phase delays [7], polarization converters [8] and other THz functional devices have become key components of these THz applications. Phase and polarization as basic parameters of electromagnetic waves can not only carry useful information, but also manipulate the propagation and states of light.

For further development of the THz application system, there is a high demand on efficient devices for guiding and manipulating THz waves in its phase and polarization. Polarization spectral analysis [9], polarization imaging [10], and polarized light communications systems [11] all require broadband, low insertion loss polarization converter. Conventional polarization optics generally depends on the birefringence of uniaxial crystalline materials [12,13]. But their birefringence is too small to satisfy the application in THz scale, for example, the birefringence of quartz crystal at 1 THz is only 0.046, and the absorption coefficient is about 0.2 cm^{-1}. The thickness of a quartz THz wave plate reaches several millimeters or even centimeters [14]. The large thickness will bring high loss, high cost and low integration, and more importantly, such wave plates can only reach a specific phase shift at a specific frequency point, and the working bandwidth is very narrow. The commonly used multilayer quartz crystal glued achromatic wave plate will further increase the device thickness and cost [15], so conventional crystal cannot meet demands of broadband THz work.

In recent years, artificial metasurfaces and sub-wavelength gratings consisting of sub-wavelength metals or dielectric units have developed rapidly [16-18]. These microstructures can easily engineer the amplitude, phase, and polarization of light to realize artificial mode birefringence, chiral polarization rotation, or dichroism by manipulating their geometries [19-23]. Compared with natural birefringence crystals, metasurfaces have the superiority in ultrathin size, easy to integrate and flexible to control. The rise of these artificial structures has brought new opportunities for the development of THz wave phase control and polarization conversion devices [24]. The metasurfaces modulates the phase of the electromagnetic wave by using the phase change caused by the electric dipole resonance of the metal subwavelength scattering unit [25]. Although the single-layer metal metallic metasurface is easy to fabricate, its polarization conversion ratio (PCR) and working bandwidth are narrow in the THz regime [26, 27].

Using multi-layer structures can significantly improve device performance. For example, in 2013, H. Chen research group at Noah Lab reported a three-layer metal wire grid THz linear polarization converter, achieving >80% conversion efficiency and near 1 THz operating bandwidth [28]. Subsequently, L.Q Cong *et al.* made a series of outstanding work on the metal substrate superficial THz polarization conversion device on a flexible substrate, and obtained a quarter waveplate (QWP) with a bandwidth greater than 0.4 THz, and first began to focus on the device's dispersion control problems [29, 30]. Capasso *et al.* and D. Tsai *et al.* reported broadband metasurface for phase control or polarization convertor in the visible light range [31-33]. However, higher reflection and Drude loss of multi-layer metal structures results in lower transmission efficiency of these devices, making it difficult to use in transmissive THz systems.

Compared with metallic structures, all-dielectric subwavelength gratings have obvious advantages in terms of transmittance. For example, S. Saha *et al.* fabricated THz silicon gratings to achieve a 1.5 THz QWP and use the SU8 anti-reflection layer to increase the transmittance by 21% [34]. However, conventional equal-period sub-wavelength gratings can only achieve a specific phase delay at a single frequency and hardly obtain a broadband wave plate.

In this paper, broadband phase shift engineering method for THz waves has been proposed based on subwavelength rectangular scattering units in the dielectric metasurface. We designed and fabricated two waveplates on high resistance silicon substrates using silicon deep etching, and experimentally confirmed that one of the structures can achieve a phase delay of about 180° in the range of 0.67-1.35 THz to achieve the function of a broadband half waveplate (HWP), and the other structure can achieve a QWP from 0.7 to 0.85 THz.

2. Structure and design

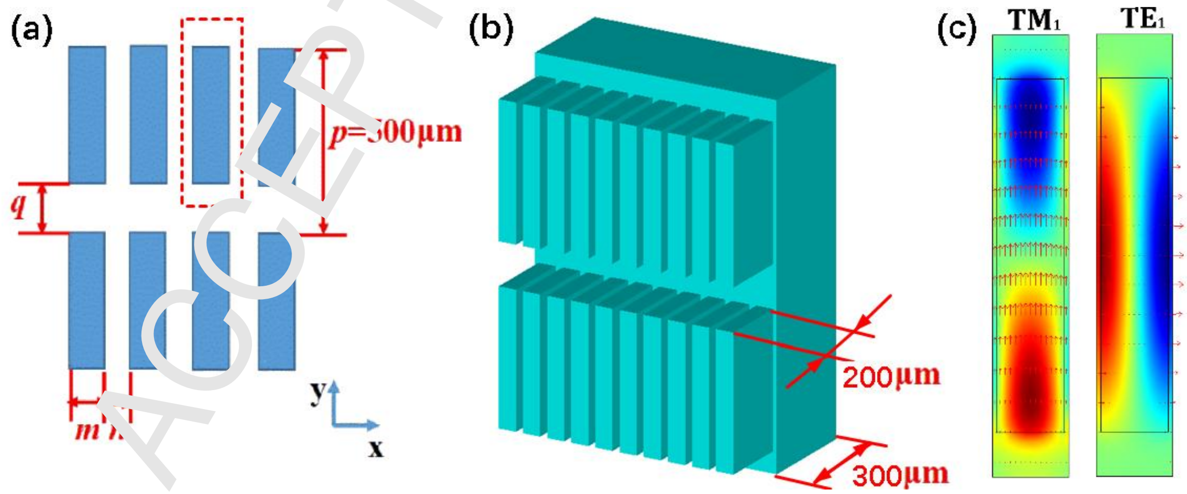

Figure.1 The schematic diagram of the device structure: (a) The top view and (b) 3D view of dielectric metasurface. (c) Simulative field distributions of fundamental TM and TE eigenmode in the metasurface.

The schematic diagram of the dielectric metasurface we proposed is shown in Figs. 1(a) and 1(b), which consists of rectangular dielectric scattering elements. The period along *x* direction is *m*+*n* and along *y* direction is fixed at *p*=500μm. The blue part is the rectangular scattering unit of silicon, of which width is *m*; the white part is the air slot, of which width is *n* along *x* axis and *q* along *y* axis; the thickness of rectangular scattering unit is 200μm, and the silicon substrate thickness is 300μm.

In order to better analyze the birefringence and phase shift characteristics of the metasurface, we use the finite element method (FEM) to simulate the eigen mode field distribution by COMSOL, and the effective refractive index of each eigen mode can be given by this simulation software. We build the structure model of *q*=120 μm, *m*=50 μm, and *n*=20 μm with a pair of periodic boundaries as shown in Fig. 1(a). The FEM results are shown in Fig. 1(c) that is the electric field distributions of the fundamental TM and TE modes at 0.9 THz. The red and blue colors represent the positive and negative normalized amplitudes of electric fields, respectively; the arrows show the polarization direction of the waves. The mode patterns indicate they are both dipole resonances with the polarization direction along *y* axis for TM mode and along *x* axis for TE mode, respectively. The birefringence of the metasurface is the difference between the effective refractive index of the TE and TM modes $\Delta n = n_{TM} - n_{TE}$, which mainly originates from the asymmetric geometry of the metasurface scattering unit along *x* and *y* direction. The phase shift of the structure is the phase difference between TM and TE modes expressed as follows:

$$\Delta\varphi(\omega) = \varphi_{\mathrm{TM}}(\omega) - \varphi_{\mathrm{TE}}(\omega) = \Delta n(\omega)\omega d / c \quad (1)$$

where $\varphi_{TE\ or\ TM}$ is the phase of the TE or TM mode, d is the total thickness of the device, c is the speed of light in vacuum, and ω is the circular frequency of THz wave.

Designing a broadband wave plate requires that the birefringence phase shift of the structure should not be significantly dependent on the frequency over a wide frequency band, that is, it has a characteristic of zero dispersion phase shift. We used the single variable method to simulate and analyze the principle of the phase shift of the metasurface by using the time domain solver of CST Microwave Studio. Figure 2 shows the influence of different structural parameters on the phase shift curve. The curves show positive dispersion in the low frequency range and negative dispersion in the high frequency. Under the certain structural parameters, there is a band with a relatively flat phase shift between the positive dispersion and the negative dispersion bands, which is just the zero-dispersion phase shift band.

The changes in dispersion of phase shift originate from the guided mode resonances in periodic scattering structures of the metasurface [35-38]. The mode patterns of these resonances are shown in Fig. 1(c). The strong resonance leads to the anomalous dispersion in phase. Due to the artificial birefringence between TE and TM polarization, the resonance position and strength of them are different, so the band of zero dispersion phase shift can be present by the superposition of the positive dispersion in TE phase and negative dispersion in TM phase with the proper geometries.

Through the structural design, the birefringence phase shift may be effectively uniform over a wide range of frequencies, which is determined by two factors. Frist, the artificial birefringence (or phase shift) comes from the anisotropic geometry in the metasurface in two orthogonal directions, so the asymmetry of scattering element m/(*p*-*q*) mainly determines the value of artificial birefringence. The *m* mainly determines the asymmetric rate *m*/*p*-*q* of scattering element when the value of long side *p*-*q* is fixed, the larger m makes the larger phase shift. As shown in Fig. 2(a) when we increase the rectangular width *m*, the phase shift curve in the band of >0.6THz gradually converts from positive dispersion to negative dispersion. When *m*=50μm, the zero-dispersion phase shift of 180° occurs from 0.6 to 1.1THz.

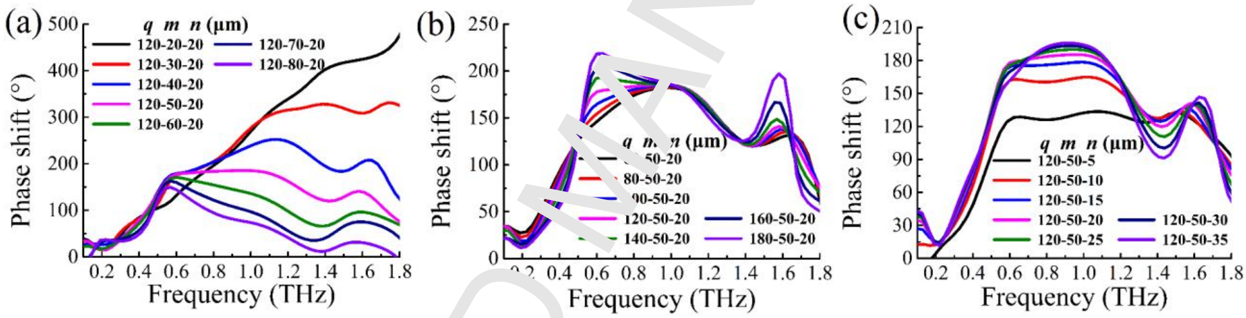

Figure. 2 Phase shift of the metasurface varying with the structure parameters. (a) Varying with *m* (width of rectangular scattering unit) when *q*=120μm and *n*=20μm; (b) Varying with *q* (the air slot width along *y* axis) when *m*=50μm and *n*=20μm; (c) Varying with *n* (the air slot width along *x* axis) when *q*=120μm and *m*=50μm.

Second, the coupling strength of resonances between adjacent scattering units is determined by the air slot width *q* and *n*. When the distance *q* and *n* between adjacent two scattering units decreases, the coupling of resonances becomes stronger. The guided mode resonance of single scattering unit becomes less prominent, and thus the phase shift curve becomes more flat without resonance valley. When the air slot width *q* along *y* direction increases as shown in Fig. 2(b), the curve gradually forms two resonances at 0.6THz and 1.6THz, which affects the flatness of the band edge of the zero-dispersion range. These resonances are just the strong guided mode resonances when the q becomes large. Figures 2(c) shows the effect of the width n of the air slot along x direction. The increase of n makes the curve becomes flatter but a lower phase shift, so selecting a proper value of n can get a certain phase shift value of the zero-dispersion band. From the above results, we can adjust the size and position of zero dispersion band and even the value of the phase shift by changing the geometric parameters. Therefore, broadband zero dispersion can be achieved by selecting suitable geometric parameters and obtaining a phase shift of 180° for HWP or 90° for QWP.

3. Fabrication and Experimental Results

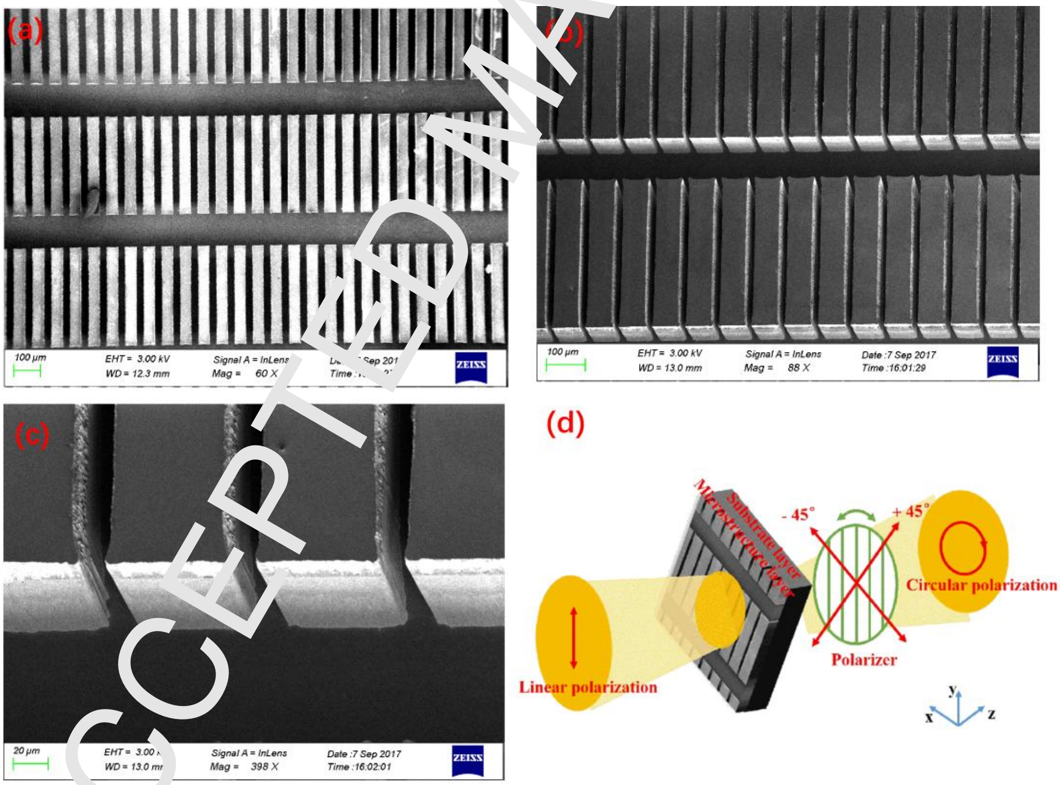

Figure.3 The SEM images of the device structure with (a) 60, (b) 88, and (c) 398 magnification. (d) Schematic diagram of the dielectric metasurface in the experimental configuration.

Based on the above design, we chose q=120 μm, m=50 μm, and n=20 μm as the optimized geometry for THz HWP. The dielectric metasurface is fabricated by the silicon deep etching in micro-electromechanical systems (MEMS) technology. A 500 μm thickness Si wafer with a high resistivity of 10 $\mathrm{K\Omega \cdot cm}$ is cleaned and a 5 μm layer of photoresist is spun onto the wafer. Then, the wafer is exposed by UV light through a designed mask to yield the expected structure, and is shaped by the inductively coupled plasma etching. The etched depth is controlled by the different etching time, about 70 min for 200 μm. Then, it is measured by a step profiler. Figure 3 shows the SEM photos of the fabricated metasurfaces.

We used the terahertz time domain spectroscopy (THz-TDS) system to measure the birefringence and polarization properties of the metasurfaces at room temperature. THz pulse is generated by a low-temperature grown GaAs photoconductive antenna (PCA). The excitation source is a Ti:sapphire laser with 75fs duration of 80MHz repetition rate at 800nm. A ZnTe crystal is used for detection. All the experiments are carried out at room temperature with the humidity of less than 5%. The detection method is shown in Fig. 3(d). The linearly polarized (LP) THz wave of which polarizing direction is along *y* axis is incident into the metasurface rotated as 45°, and time domain signals of the two orthogonal polarization components (TE and TM LP modes) can be obtained by rotating a THz polarizer behind the metasurface. The amplitude ($A_{\mathrm{TE}}(\omega)$ and $A_{\mathrm{TM}}(\omega)$) and phase ($\varphi_{\mathrm{TE}}(\omega)$ and $\varphi_{\mathrm{TM}}(\omega)$) of them can be calculated by Fourier Transform of time domain signals shown in Fig. 4(a). The phase shift can be calculated by Eq. (1) as shown in Fig. 4(b). And the effective refractive index $n_{\mathrm{TE\ or\ TM}}$ and artificial birefringence Δn can be calculated by:

$$n_{\mathrm{TE\ or\ TM}}(\omega) = \frac{[\varphi_{air}(\omega) - \varphi_{\mathrm{TE\ or\ TM}}(\omega)]c}{\omega d} + 1, \Delta n = n_{TM} - n_{TE} \qquad (2)$$

where φ_{air} is the phase of the air reference, d=500μm is the total thickness of the device.

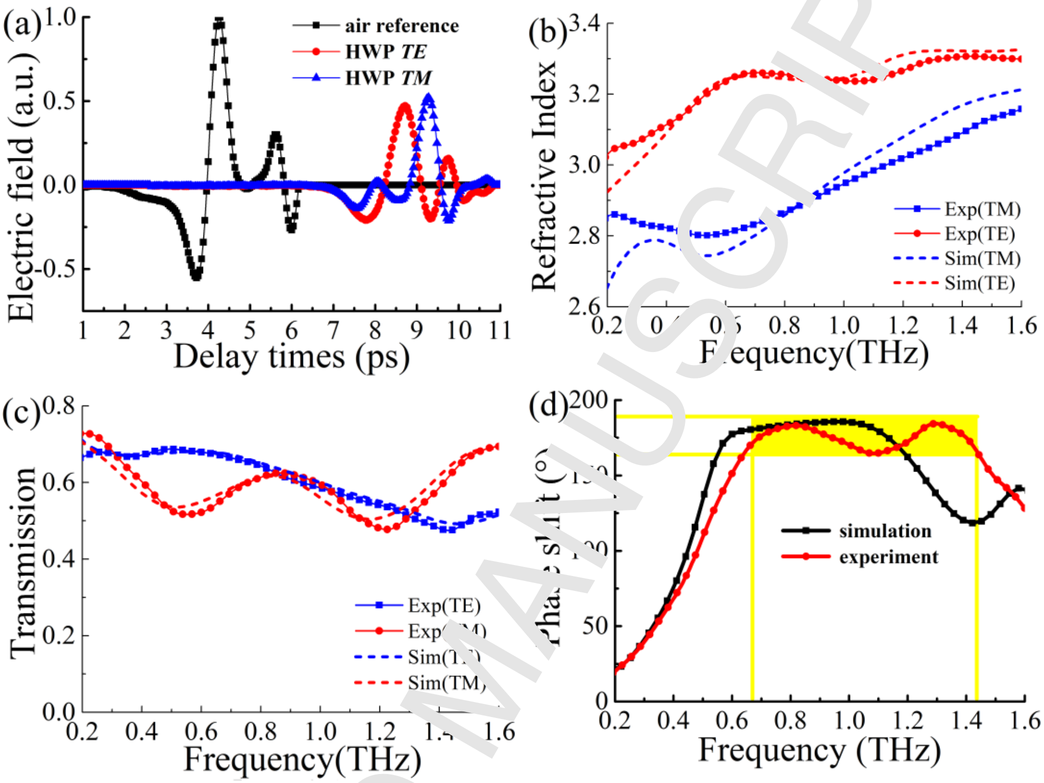

Figure.4 Birefringence and phase shift characteristics of the HWP structure. (a) Experimental time domain pulses of TE and TM modes and air reference; (b) Experimental and simulative refractive index, (c) amplitude transmission, and (d) phase shifts of TE and TM mode.

Figures 4(a) and 4(b) show the THz time-domain signals and refractive index of the TE and TM modes of the metasurface. In the range of 0.2-1.6 THz, we can see the effective refractive index of the TE mode is always smaller than the effective refractive index of TM mode, and the birefringence is over 0.4. Figures 4(c) and 4(d) show the amplitude transmission spectra and phase shift of the TE and TM modes obtained in our simulations and experiments. We can find that the two orthogonal LP components are close to each other in the broadband frequency range, and experimental results show that zero dispersion phase shift can be obtained in the range of 0.67-1.43 THz. The range of the zero dispersion phase shift is defined as the band of ±5°

deviated from 180°. In addition, the experimental results are in good agreement with the simulation results. The difference between experimental and simulated results mainly comes from machining error of the device.

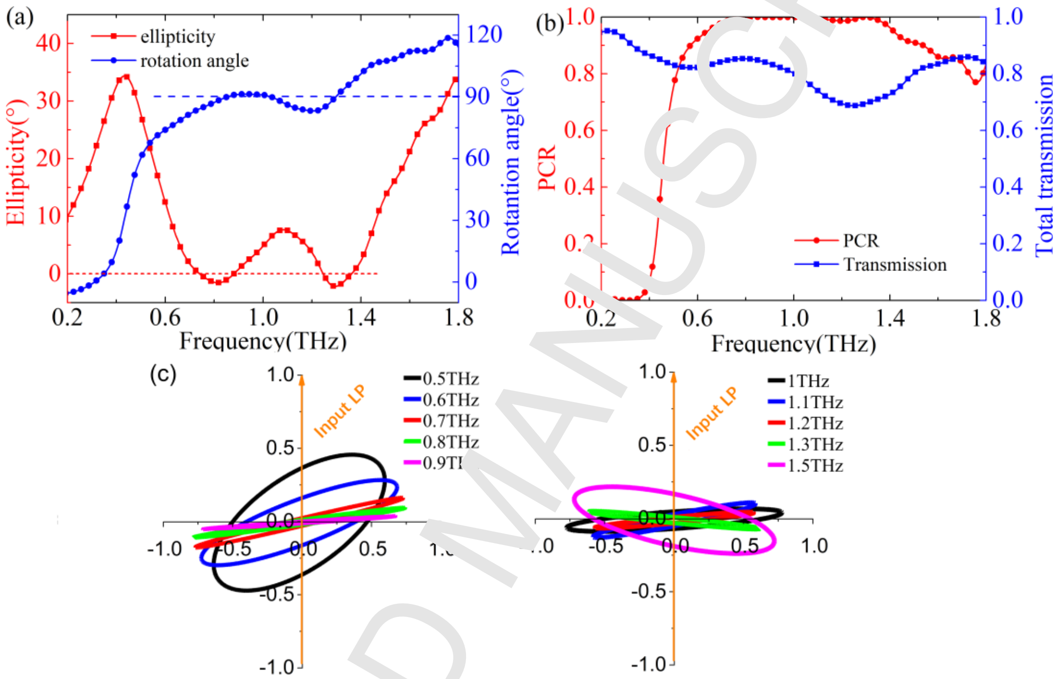

Figure. 5 Polarization conversion characteristics of the HWP structure. (a) Ellipticity and polarization rotation angle curve *v.s.* THz frequency; (b) PCR and total transmission spectra in the THz regime; (c) Polarization states of the output light vector at 0.5~1.5THz when the incident wave is a LP light along *y* axis and the metasurface is rotated at 45°.

The polarization conversion characteristics of this HWP metasurface can be further characterized by some key parameters: ellipticity ε, polarization rotation angle ψ and PCR. All these parameters can be derived from the measured amplitude $A_{TE}(\omega)$, $A_{TM}(\omega)$ and phase difference $\Delta\varphi(\omega)$:

$$\tan 2\varepsilon = \sin 2\beta \sin \Delta\varphi \tag{3}$$

$$\tan 2\psi = \tan 2\beta \cos \Delta\varphi \tag{4}$$

where $\tan\beta = A_{\mathrm{TM}} / A_{\mathrm{TE}}$. As shown in Fig. 5(a), the ellipticity and polarization rotation angle curve are calculated by Eqs. (3) and (4), respectively. ε=0 means the output light is a LP, $\varepsilon = 45^{\circ}$ means a left-handed circularly polarized light (LCP) and -45° is a right-handed circularly polarized light (RCP). ψ indicates the rotated angle to the original LP. Therefore, in the range of 0.67~0.14THz, $\varepsilon \approx 0$ and $\psi \approx 0$, the output light is close to a LP with 90° rotation angle. This metasurface can rotate a LP to 90° from y axis to x axis. The total transmittance T of this metasurface and the PCR for HWP and can be expressed as:

$$T_{total}{}^{2} = T_{y\to y}{}^{2} + T_{y\to x}{}^{2} = \frac{A_{TE}^{2}}{A_{air}^{2}} + \frac{A_{TM}^{2}}{A_{air}^{2}} \tag{5}$$

$$PCR(\text{for HWP}) = \frac{T_{y\to x}{}^{2}}{T_{y\to y}{}^{2} + T_{y\to x}{}^{2}} = (T\cos\psi)^{2} \tag{6}$$

By the above Eqs. (5) and (6), we can find that the PCR of this HWP is over 99% from 0.73 to 1.35THz, and the total transmission of the device is over 70% in this range, as shown in Fig. 5(b). Notice that all the word "transmission" in this paper means "amplitude transmission" T not "intensity transmission" T^2.

The polarization ellipse of the output light vector is expressed as

$$\frac{E_x^2}{A_{TE}^2} + \frac{E_y^2}{A_{TM}^2} - 2\frac{E_x E_y}{A_{TE} A_{TM}}\cos(\Delta\varphi) = \sin^2(\Delta\varphi) \tag{7}$$

The results are drawn in Fig. 5(c), and we can visually see that the LP light along y axis is rotated to the x axis, remaining a close LP state from 0.7 to 1.3THz. Therefore, this structure can achieve linear polarization conversion with a phase shift of about 180° in a bandwidth of 0.66 THz, thereby effectively realizing the function of the broadband HWP.

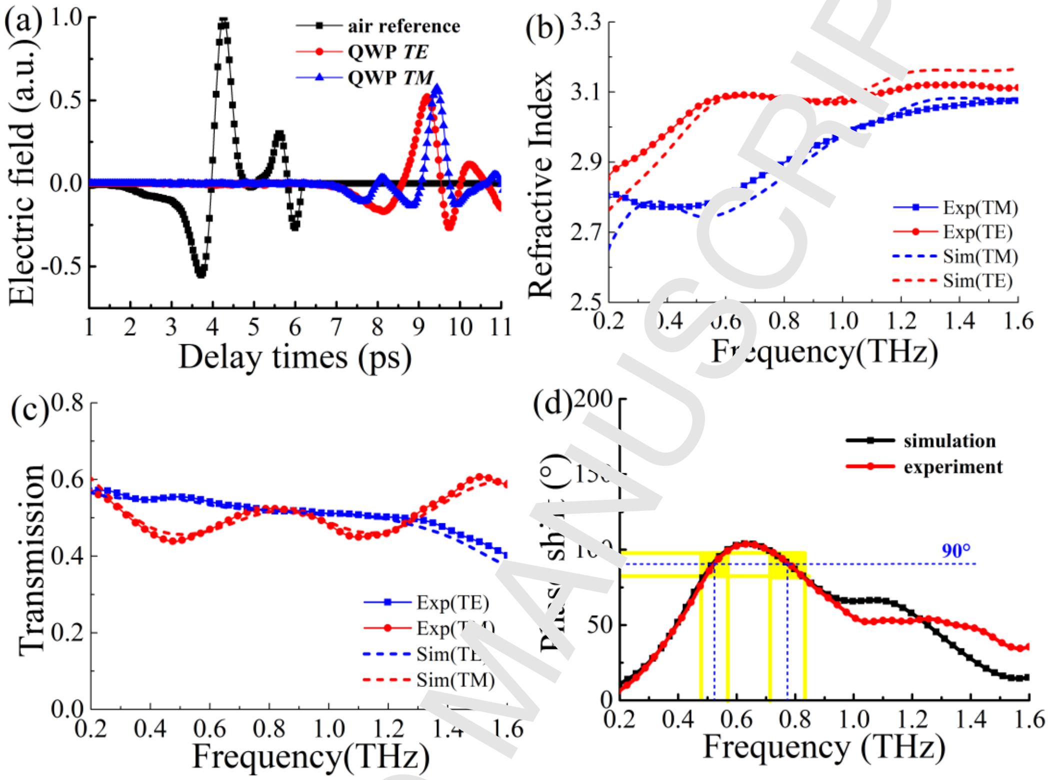

Figure.6 Birefringence and phase shift characteristics of the QWP structure. (a) Experimental time domain pulses of TE and TM modes and air reference; (b) Experimental and simulative refractive index, (c) amplitude transmission, and (d) phase shifts of TE and TM mode.

Similar to the HWP, we selected the appropriate structural parameters and fabricated the QWP in the same way. Structural parameters q=100μm, m=76μm, and n=10μm. The experiment and simulation results are shown in Fig. 6, and the experimental results also fit well with the simulation results. In the range of 0.2-0.6 THz, the birefringence coefficient increases monotonically with frequency and decreases in 0.6-1.6 THz. The structure can achieve phase shift of about 90° from 0.5 to 0.85 THz. In this range, the LP light can be converted into a circularly polarized light by this THz QWP metasurface.

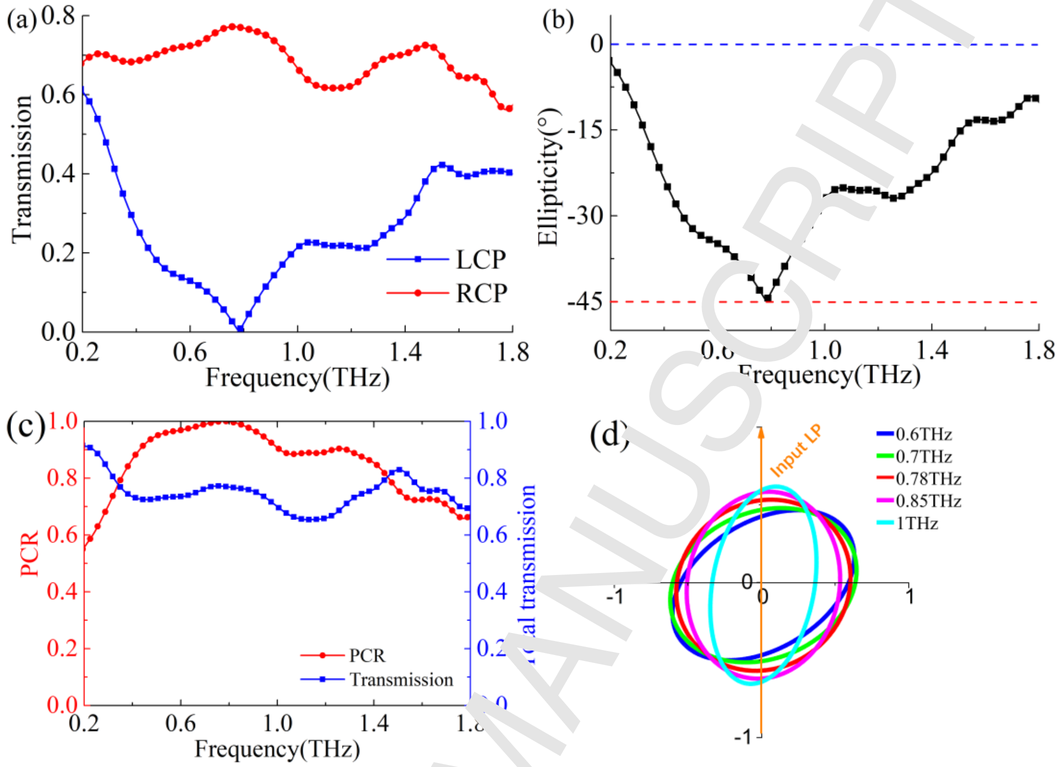

Figure. 7 Polarization conversion characteristics of the HWP structure. (a) The transmission spectra of LCP and RCP components calculated by the experimental TE and TM LP components. (b) Ellipticity curve *v.s.* THz frequency; (c) PCR and total transmission spectra in the THz regime; (c) Polarization states of the output light at different THz frequency from 0.6 to 1THz when the incident wave is a LP light along *y* axis and the metasurface is rotated as 45°.

The polarization conversion characteristics of this QWP metasurface are also derived by experimental data. Different from the orthogonal LP conversion of HWP, the PCR should be defined by the transmission of the output LCP light or RCP light, which is expressed as

$$\begin{aligned} T_{total}{}^2 &= T^2_{\mathrm{LCP}} + T^2_{\mathrm{RCP}} = T^2_{\mathrm{TE}} + T^2_{\mathrm{TM}} \\ PCR(\text{for QWP}) &= \frac{T^2_{\mathrm{LCP\ or\ RCP}}}{T_{total}{}^2}, \end{aligned} \tag{8}$$

where the measured orthogonal TM and TE LP components can be equivalently transformed as the forms of the orthogonal LCP and RCP components as follows:

$$T_{RCP}=\left|\frac{1}{\sqrt{2}}(A_{TE}e^{i\varphi_{TE}}+iA_{TM}e^{i\varphi_{TM}})\right|/A_{air}$$
$$T_{LCP}=\left|\frac{1}{\sqrt{2}}(A_{TE}e^{i\varphi_{TE}}-iA_{TM}e^{i\varphi_{TM}})\right|/A_{air} \quad (9)$$

By these equations, we can find that the RCP is much higher than the LCP, especially at 0.78THz as shown in Fig. 7(a). And Fig. 7(b) shows that $\varepsilon=-45^{\circ}$ at 0.78THz, which also indicate this is a perfect RCP light. The PCR is over 90% from 0.7 to 0.85THz, reaching 99.5% at 0.78THz. And the transmission of this QWP metasurface is over 70% in this frequency range, as shown in Fig. 7(c). Finally, we also show the polarization ellipse of the output light vector in Fig. 7(d), which shows that the good circles are obtained at 0.7THz, 0.78THz, and 0.85THz, especially to be perfect at 0.78THz. Therefore, this metasurface can work as a broadband THz QWP from 0.7 to 0.85THz.

4. Conclusion

In summary, broadband THz phase shift engineering and zero-dispersion waveplates based on dielectric metasurface have been investigated. By designing the proper geometric parameters of the metasurface structure, the value, dispersion and bandwidth of the birefringence phase shift can be effectively manipulated. Based on this, we designed and fabricated the THz broadband HWP and QWP metasurfaces. The results show that the HWP can work in the broad range of 0.67-1.35 THz with the PCR of close to 100% and the transmission of over 70%. And the QWP can operate in the range of 0.7~0.85THz with the PCR of over 90% and the transmission of over 70%. The method of phase shift engineering based on dielectric metasurfaces and these broadband zero-dispersion waveplates have great potential in promoting the performance of THz application systems.

Acknowledgments

This work was supported by National Key Research and Development Program of China (2017YFA0701000); National Natural Science Foundation of China (61831012, 61671491); Young Elite Scientists Sponsorship Program by Tianjin (TJSQNTJ-2017-12).

References

1. R. A. Kaindl, M. A. Carnahan, D. Hägele, R. Lövenich, D. S. Chemla, "Ultrafast terahertz probes of transient conducting and insulating phases in an electron-hole gas" Nature 6941 (2003) 734-738.
2. M. Nagel, P. Haring Bolivar, M. Brucherseifer, and H. Kurz, "Integrated THz technology for label-free genetic diagnostics" Appl. Phys. Lett. 80 (2002) 154-156.
3. B. B. Hu, M. C. Nuss, "Imaging with terahertz waves." Opt. Lett. 20(16) (2002) 1716-1718.
4. T. Kleine-Ostmann, T. Nagatsuma, "A review on terahertz communications research" Infrared Milli. Terahertz Waves. 32 (2011) 143-171.
5. S. Chen, F. Fan, Y. Miao, X. He, K. Zhang, and S. Chang, "Ultrasensitive terahertz modulation by silicon-grown MoS2 nanosheets" Nanoscale 8 (2016) 4713-4719.
6. S. F. Busch, S. Schumann, C. Jansen, M. Scheller, M. Koch, B. M. Fischer, "Optically gated tunable terahertz filters" Appl. Phys. Lett. 100 (2012) 261109.
7. M. Chen, F. Fan, S.T. Xu, S.J. Chang, "Artificial high birefringence in all-dielectric gradient grating for broadband terahertz waves" Sci. Rep. 6 (2016) 38562.
8. L. Ren, C. L. Pint, T. Arikawa, K. Takeya, I. Kawayama, "Broadband terahertz polarizers with ideal performance based on aligned carbon nanotube stacks" Nano Lett. 12 (2012) 787-790.

9. T. Nagashima, M. Tani, M. Hangyo, “Polarization-sensitive THz-TDS and its application to anisotropy sensing” J. Infrared Millim. 34 (2013) 740–775.

10. P. Doradla, K. Alavi, C. Joseph, R. Giles, and J. Biomed. “Detection of colon cancer by continuous-wave terahertz polarization imaging technique” J. Biomed. Opt. 18(9) (2013) 090504.

11. T. Nagatsuma, G. Ducournau, and C. C. Renaud, “Advances in terahertz communications accelerated by photonics” Nat. Photon. 10 (2016) 371–379.

12. K. Wiesauer and C. J¨ordens, “Recent advances in birefringence studies at THz frequencies” J. Infrared Millim. 34 (2013) 663–681.

13. A. K. Kaveev, G. I. Kropotov, E. V. Tsygankova, I. A. Tzibizov, S. D. Ganichev, S. N. Danilov, P. Olbrich, C. Zoth, E. G. Kaveeva, A. I. Zhdanov,A. A. Ivanov, R. Z. Deyanov, and B. Redlich, “Terahertz polarization conversion with quartz waveplate sets” Appl. Opt. 52 (2013) B60-B69.

14. D. Grischkowsky, S. Keiding, M. V. Exter, C. Fattinger, “Far-infrared time-domain spectroscopy with terahertz beams on dielectrics and semiconductors” J. Opt. Soc. Am. B. 10 (1990) 2006-2015.

15. J. B. Masson, G. Gallot, “Terahertz achromatic quarter-wave plate” Opt. Lett. 31 (2006) 265–267.

16. N. I. Zheludev, Y. S. Kivshar, “From metamaterials to metadevices” Nat. Mater. 11 (2012) 917–924.

17. D. M. Lin, P. Y. Fan, E. Hasman, M. L. Brongersma, “Dielectric gradient metasurface optical elements” Science 345 (2014) 298–302.

18. S. K. Lee, B. Kang, H. Keum, N. Ahmed, J. A. Rogers, P. M. Ferreira, S. Kim, and B. Min, “Heterogeneously assembled metamaterials and metadevices via 3D modular transfer printing” Sci. Rep. 6 (2016) 27621.

19. L. Q. Cong, P. Pitchappa, Y. Wu, L. Ke, C. Lee, N. Singh, H. Yang, and R. Singh, “Active multifunctional microelectromechanical system metadevices: applications in polarization

control, wavefront deflection, and holograms" Adv. Opt. Mater. 5 (2017) 1600716.

20. S. Liu, T. J. Cui, Q. Xu, D. Bao, L. Du, X. Wan, W. Tang, C. Ouyang, X. Y. Zhou, H. Yuan, H. F. Ma, W. X. Jiang, J. Han, W. Zhang, and Q. Cheng, "Anisotropic coding metamaterials and their powerful manipulation of differently polarized terahertz waves" Light: Sci. Appl. 5 (2016) e16076.
21. C. Huang, Y. Feng, J. Zhao, Z. Wang, and T. Jiang, "Asymmetric electromagnetic wave transmission of linear polarization via polarization conversion through chiral metamaterial structures" Phys. Rev. B 85 (2012) 195131.
22. R. H. Fan, Y. Zhou, X. P. Ren, R. W. Peng, S. C. Jiang, D. H. Xu, X. Xiong, X. R. Huang, and M. Wang, "Freely tunable broadband polarization rotator for terahertz waves" Adv. Mater. 27 (2015) 1201.
23. Z. J. Wang, H. Jia, K. Yao, W. S. Cai, H. S. Chen, and Y. M. Liu, "Circular dichroism metamirrors with near-perfect extinction" ACS Photon. 3 (2016) 2096-2101.
24. L. Zhang, S Mei, K. Huang, C. W. Qiu, "Advances in full control of electromagnetic waves with metasurfaces" Adv. Opt. Mater. 4(6) (2016) 818-833.
25. Q. L. Cong, N. N. Xu, W. L. Zhang, R Singh, "Polarization control in terahertz metasurfaces with the lowest order rotational symmetry" Adv. Opt. Mater. 3(9) (2015) 1176-1183.
26. W. W. Liu, S. Q. Chen, Z. C. Li, H. Cheng, P. Yu, J. X. Li, and J. G. Tian, "Realization of broadband cross-polarization conversion in transmission mode in the terahertz region using a single-layer metasurface" Opt. Lett. 40 (2015) 3185–3188.
27. D. C. Wang, Y. H. Gu, Y. D. Gong, C. W. Qiu, and M. H. Hong, "An ultrathin terahertz quarter-wave plate using planar babinet-inverted metasurface" Opt. Express. 23 (2015) 11114–11122.
28. N. K. Grady, J. E. Heyes, D. R. Chowdhury, Y. Zeng, M. T. Reiten, A. K. Azad, A. J. Taylor, D. A. R. Dalvit, H. T. Chen, "Terahertz metamaterials for linear polarization conversion and anomalous refraction" Science 361 (2013) 1304.
29. Q. L. Cong, N. N. Xu, Q. J. Gu, R. Singh, G. J. Han, W. L. Zhang, "Highly flexible

broadband terahertz metamaterial quarter‐wave plate” Laser & Photon. Rev. 8 (2014) 626-632.

30. Q. L. Cong, N. N. Xu, Q. J. Gu, J. G. Han, W. L. Zhang, R. Singh, “A tunable dispersion-free terahertz metadevice with Pancharatnam-Berry-Phase-Enabled modulation and polarization control” Adv. Mat. 27 (2015) 6630-6636.

31. N. Yu, F. Aieta, P. Genevet, M.A. Kats, Z. Gaburro, F. Capasso, “A broadband, background-free quarter-wave plate based on plasmonic metasurfaces” Nano Lett. 12(12) (2012) 6328-6333.

32. P. C. Wu, W. Zhu, Z. X. Shen, P. Chong, W. Ser, D. P. Tsai, “Broadband wide-angle multifunctional polarization converter via liquid-metal-based metasurface” Adv. Opt. Mater. 5(7) (2017) 1600938.

33. W .T. Chen, K. Y. Yang, C. M. Wang, Y. W. Huang, G. Sun, I. D. Chiang, C. Y. Liao, W. L. Hsu, H. T. Lin, S. Sun, L. Zhou, A. Q. Liu, D. P. Tsai, “High-efficiency broadband meta-hologram with polarization-controlled dual images” Nano Lett. 14(1) (2013) 225-230.

34. S. C. Saha, Y. Ma, J. P. Grant, A. Khalid, D. R. S. Cumming, “Low-loss terahertz artificial dielectric birefringent quarter-wave plates” IEEE Photon. Tech. Lett. 22(2) (2010) 79-81.

35. S. Fan and J. Joannopoulos, "Analysis of guided resonances in photonic crystal slabs," Phys. Rev. B 65 (2002) 235112.

36. P. Pottier, L. Shi, and Y. A. Peter, "Determination of guided-mode resonances in photonic crystal slabs," J. Opt. Soc. Am. B 29 (2012) 109-117.

37. T. Prasad, V. L. Colvin, and D. M. Mittleman, "The effect of structural disorder on guided resonances in photonic crystal slabs studied with terahertz time-domain spectroscopy," Opt. Exp. 15 (2007) 16954-16965.

38. F. Fan, S. Chen, X. H. Wang, P. F. Wu, and S. J. Chang, “Terahertz refractive index sensing based on photonic column array,” IEEE Photonic. Tech. Lett. 27 (2015) 478-481.